RSC Advances

PAPER

View Article Online
View Journal | View Issue

Cite this: *RSC Adv.*, 2024, **14**, 36005

Effect of magnetic field on the rate performance of a Fe_2O_3/$LiFePO_4$ composite cathode for Li-ion batteries†

Emmanuel Iheonu Nduka, ‡[a] Nazgul Assan, ‡[a] Mukagali Yegamkulov,[b] Aliya Mukanova [ab] and Zhumabay Bakenov *[abc]

Received 17th September 2024
Accepted 28th October 2024

DOI: 10.1039/d4ra06707j

rsc.li/rsc-advances

Lithium iron phosphate ($LiFePO_4$ or LFP) is a widely used cathode material in lithium-ion batteries (LIBs) due to its low cost and environmental safety. However, LFP faces challenges during high-rate operation and prolonged cycling. Magnetic field (MF) can enhance ionic conductivity and reduce polarization in the LFP cathode, particularly when magnetically sensitive iron oxide is added to the cathode. In this study, $LiFePO_4$ was optimized by simply adding Fe_2O_3 (FO) nanoparticles and drying the composite cathode (FO/LFP) with and without applying MF. Electrochemical tests demonstrated that the optimized samples prepared at two concentrations of Fe_2O_3 (1 wt% and 3 wt%) exhibited improved electrochemical characteristics and inhibited polarization upon operation. Lithium-ion diffusion coefficient calculations revealed an increase in this value in the case of the MF-assisted samples compared to their non-MF counterparts. The 1 wt% FO/LFP cathode dried under an MF showed noticeably high reversible capacity, slow capacity decay, and enhanced rate capability, especially when cycled at a high current density of 5C. This research successfully demonstrated a relatively facile method to improve the rate performance of $LiFePO_4$ cathodes that can be easily incorporated into the large-scale battery production.

1. Introduction

Lithium-ion batteries (LIBs) have become the base of modern energy storage systems, powering everything from handheld gadgets to electric vehicles and grid-scale energy storage systems, due to their low maintenance, high power, excellent performance, and longevity.[1–3] Among LIB cathodes, lithium iron phosphate ($LiFePO_4$) is regarded as one of the most widely used cathode materials. Nevertheless, its drawbacks include relatively low operating potential, insufficient rate performance, weak electron conductivity, low Li ion diffusion coefficient, and low volumetric specific capacities across electrodes, making $LiFePO_4$ an unviable cathode material from an economic standpoint.[2–7] To overcome these challenges, many efforts have relied on internal strategies, such as modifying or optimizing the cell components *via* coating and doping, morphological control, and particle size reduction.[6,8–10] Although these strategies could improve the electrochemical performances, they still have their advantages and disadvantages. For instance, increased surface area necessitates using more binders during electrode fabrication, which increases cell polarization. Moreover, a decrease in the particle size reduces the tap density, and the actual role of metal doping has been complicated and contentious thus far.[11,12] There is another effective technique of applying an external force, for example magnetic field (MF), which is able to affect the electrochemical characteristics of LIBs. It was shown that the Li ion diffusion in $LiFePO_4$ primarily occurs through one-dimensional channels along the crystal *b*-axis (010). However, by controlling the particle shape based on anisotropy, which significantly influences the crystal growth, $LiFePO_4$ can achieve a high rate of Li^+ diffusion, thereby enabling excellent performances in $LiFePO_4$ batteries.[13,14] According to Gao *et al.*, when an MF is imposed perpendicular to an electrode surface, the tiny crystals align along the *b*-axis coordinate (010), with the half-cell's operating direction, thereby increasing Li^+ diffusion along the channel.[1] Another research demonstrated that when an MF is applied in the synthetic process of electrode materials, the nucleation and growth processes shift, resulting in anisotropy and modifying the crystal lattice, thereby decreasing the surface energy, directional expansion along the easy axis and increasing dipoles.[15] Further, it was shown that when magnetic moments of materials are exposed to an MF, they exhibit a precise level of magnetism known as magnetization, modifying the crystal orientation and boosting the high-rate and cycling performance

[a]*Department of Chemical and Materials Engineering, School of Engineering and Digital Sciences, Nazarbayev University, Astana 010000, Kazakhstan. E-mail: zbakenov@nu.edu.kz*

[b]*National Laboratory Astana, Nazarbayev University, Astana 010000, Kazakhstan*

[c]*Institute of Batteries LLC, Nazarbayev University, Astana 010000, Kazakhstan*

† Electronic supplementary information (ESI) available. See DOI: https://doi.org/10.1039/d4ra06707j

‡ These authors contributed equally.

in LIBs.[16] For example, Zhou *et al.* aligned $LiFePO_4$ monocrystalline platelets along the *b*-axis to enhance high-rate performance and increase Li^+ diffusion coefficients, which boosted the capacity for rapid discharge using a 0.5 T MF.[4] C. Kim *et al.* investigated the magnetism and magnetic susceptibility of $LiFePO_4$, demonstrating lower electrode polarization and higher reversible capacity using a 6 T superconducting magnet system.[5]

Although the MF shows a positive effect towards better performance in LIBs, the use of magneto-sensitive additives such as iron-based oxides (α-Fe_2O_3) is being investigated as a promising approach to enhance this effect and obtain even better electrochemical, magnetic, and structural characteristics of LIB electrodes.[17,18] In the synthesis of $LiFePO_4$, Fe_2O_3 (FO) has been seen as a promising magnetic-sensitive nanoparticle (MNP) due to its abundance, chemical stability, high theoretical specific capacity, low cost, and environmentally friendly attributes.[19] Liu *et al.* synthesized a $LiFePO_4$/C cathode material using Fe_2O_3, which showed excellent capacity retention and reversibility with 145.8 mA h g^{-1} at 0.2C.[17] Wang *et al.* synthesized $LiFePO_4$/C composites by a carbothermal reduction method using Fe_2O_3 as an iron source, and the maximum discharge capacity (156 mA h g^{-1}) was achieved using sucrose as a carbon source at 0.1C.[20] Further, Ho-Ming *et al.* applied γ-Fe_2O_3 at different concentrations to prepare $LiFePO_4$ composite cathodes, and among them, the electrode containing 15 wt% γ-Fe_2O_3 demonstrated a high average specific discharge capacity at a cycling rate of 10C.[21] This suggests that incorporating Fe_2O_3 into the electrode during slurry preparation offers a simple and less expensive strategy to enhance the power density and cycling life of LIBs.

Hence, to solve the above-mentioned issues, we conducted an experimental study to assess how MF and magnetically responsive Fe_2O_3 nanoparticles affect the performance of fast-charging LIBs. Specifically, we used a permanent magnet with an intensity of 0.3 T solely during the fabrication of the cathode slurry. In contrast to the results of previous reports,[4,5] where a monocrystalline active material ($LiFePO_4$) was synthesized and aligned along the *b* axis *via* magnetic orientation to investigate the rate performance of $LiFePO_4$, we employed a polycrystalline commercial $LiFePO_4$ active material and mixed it with Fe_2O_3 MNPs during slurry preparation, and the thus-prepared slurry was dried on a permanent 0.3 T magnet. We believe that utilizing MF with a moderate intensity of 0.3 T makes it easy to incorporate the investigated process into the LIB plants with large production lines, which along with the use of commercial polycrystalline LFP makes this process attractive for practical applications.

2. Materials and methods

2.1. Chemicals and instruments

Commercial lithium iron phosphate ($LiFePO_4$, purity 99.9%, MTI Corporation, USA) was used as an active material, acetylene black (AB, purity 99.9%, MTI Corporation, USA) with a net weight of 50 g per bottle was used as a conductive substance, and iron(III) oxide was used as magnetic-sensitive nanoparticles (dispersion nanoparticles, Sigma-Aldrich, Co., USA). The binder was polyvinylidene fluoride with a net weight of 1100 kg mol^{-1} (PVDF, purity 99.5%, MTI Corporation, USA). The solvent was *N*-methyl 2-pyrrolidone (NMP, purity 99.8%, Sigma-Aldrich, Co., USA). Before slurry preparation, the active material, PVDF, and

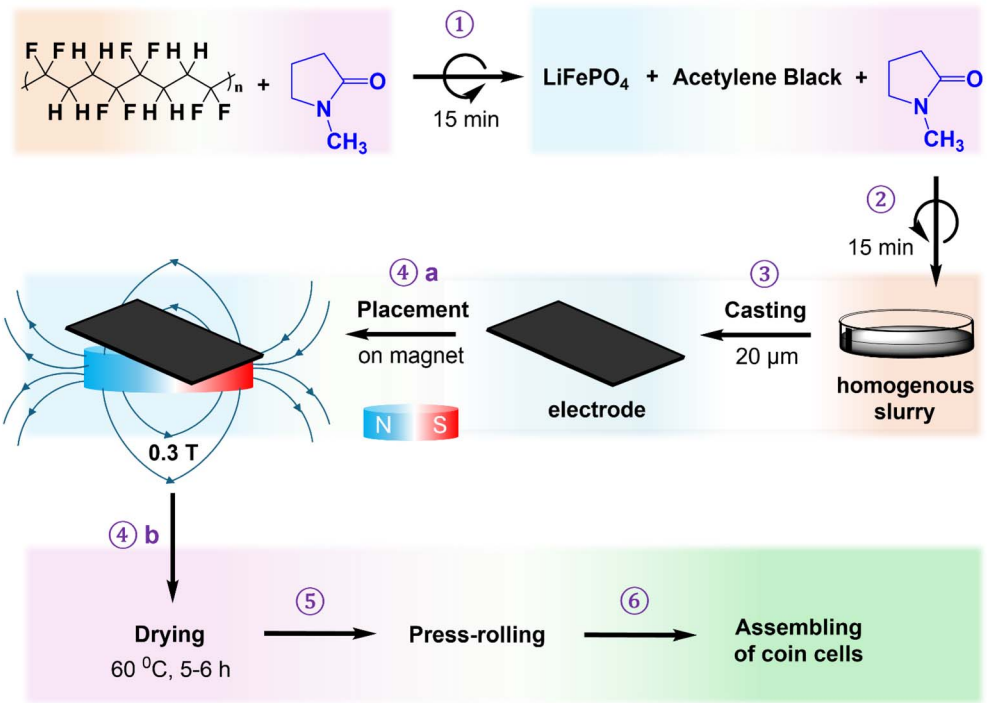

Scheme 1 Cathode preparation procedure.

conductive additives were pre-dried in a vacuum oven at 60 °C for 12 hours to minimize the residual moisture content.

A neodymium magnet (diameter: 70 mm; thickness: 40 mm) with an intensity of 0.3 T (Astana, Kazakhstan) was used during the electrode drying process.

2.2. Sample characterization

The crystal and phase structures of the prepared electrode materials were determined by X-ray diffraction (XRD, MiniFlex benchtop, Rigaku Co., Japan) with Cu Kα radiation (λ = Kα = 1.541862 Å) at 2θ in the range from 10° to 70° at a scanning speed of 1° min^{-1}. The electrodes were fabricated by a doctor blade technique using an Al foil current collector and dried for 6 hours with and without MF. The dried samples were punched into circular electrodes of 14 mm diameter.

Two types of scanning electron microscopes (SEM, JSM-7500F JEOL, Japan, and Crossbeam 540, ZEISS, Germany) were used to analyze the sample particle size, morphology, and thickness. To analyze the average thickness of each electrode, a total of 100 points were measured for each of the electrode samples using the JMicroVision software (v1.3.4), as shown in Fig. S3a (ESI).† This process was repeated five times for all electrodes to ensure the accuracy and reliability of the measurements. Further, transmission electron microscopy (TEM, JEM-1400 plus, JEOL, Japan) was performed to determine the particle size of Fe_2O_3 (FO).

2.3. Preparation and characterization of Fe_2O_3

First, 25 mL of Fe_2O_3 nanoparticle dispersion was placed in a vial and subjected to drying using a freeze dryer (Labconco, Co., USA) at −50 °C under reduced pressure (10 Pa) for two days. The resulting yellow-colored FO nanoparticle powder was transferred to a plastic tube for storage. The nanoparticles were stored at 60 °C in a vacuum oven to prevent moisture effects and potential degradation. To determine the particle size of FO, 5 mg of FO was diluted in 5 mL of ethanol, and the solution was dropped onto a holey carbon support film-coated Cu microgrid (Ted, Pella, Inc., USA). Within 5 minutes, the grid was transferred to a vacuum oven and dried overnight. Then, the grid underwent hydrophilic treatment in a glow discharge irradiation chamber and used for TEM investigations at an accelerating voltage of 80 kV. To analyze the average particle size, 100 points were measured for each TEM image analysis using the JMicroVision software (v1.3.4), as shown in Fig. S3b (ESI).† This process was repeated five times for all images to ensure the accuracy and reliability of the measurements.

2.4. Cathode preparation

The cathode slurries consisted of $LiFePO_4$, PVDF, AB, and Fe_2O_3 prepared in weight ratios of 80 : 10 : 10 : 0, 80 : 10 : 9 : 1, and 80 : 10 : 7 : 3 in 600 μL *n*-methyl pyrrolidone solvent (NMP). The slurries were mixed using planetary centrifugal vacuum mixers (ARV-310CE, Japan) at 1200 rpm and under 98.2 kPa for 15 minutes. The samples were mixed into two cycles (30 minutes total) to achieve homogenous distribution of the slurry components (Scheme 1, steps 1 and 2). The slurry was then coated onto an Al foil current collector with a 20 μm doctor blade (Scheme 1, step 3), placed on a magnet of 0.3 T (Scheme 1, step 4a), and dried at 60 °C under vacuum for 6 hours to obtain

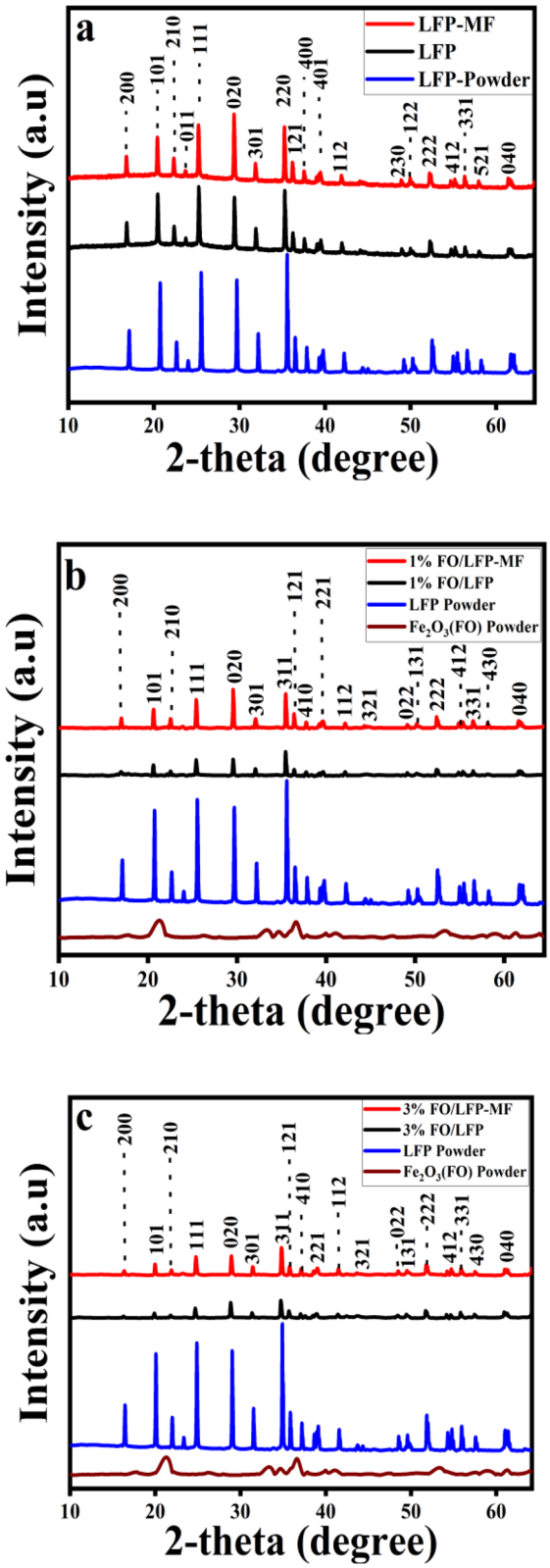

Fig. 1 XRD patterns of the cathodes: (a) LFP and LFP-MF; (b) 1% FO/LFP and 1% FO/LFP-MF; and (c) 3% FO/LFP and 3% FO/LFP-MF.

a uniformly dispersed cathode (Scheme 1, step 4b), denoted as LFP-MF, 1% FO/LFP-MF, and 3% FO/LFP-MF, respectively. The reference slurries were dried without a magnet to produce a naturally distributed cathode labeled as LFP, 1% FO/LFP, and 3% FO/LFP, respectively.

2.5. Electrochemical cell assembly and electrochemical characterization

The dried cathodes were roll-pressed using a calendaring machine (Nonheating WCRP-1015G, Hohsen Co., Japan) and punched into disks of 14 mm diameter, which were used for electrochemical tests. The electrochemical properties of the electrodes were evaluated in CR2032 coin-type cells (Hohsen Co., Japan), which were assembled in an Ar-filled glovebox (oxygen and water <0.1 ppm, LabMaster, Mbraun, Germany). The separator and electrolyte were polypropylene membrane (Celgard 2400) and 1 M $LiPF_6$ in ethylene carbonate and dimethyl carbonate (DMC : EC, 1 : 1 v/v), respectively, with a lithium metal chip as a reference and counter electrode. The cyclic voltammogram (CV) measurements were performed at room temperature on a VMP3 potentiostat/galvanostat (Biologic Inc., France) at different scan rates ranging within 0.1–0.5 mV s^{-1} from 2.8 to 4.2 V *vs.* Li/Li^+. Galvanostatic charge/discharge cycling was carried out at cutoff potentials 2.8 to 4.2 V *vs.* Li/Li^+ at various cycling rates from 0.1 to 5C using a Neware battery tester (Neware Co., China). AC electrochemical impedance spectroscopy (EIS) was performed using a potentiostat/galvanostat within a frequency range of 100 kHz to 0.1 Hz and

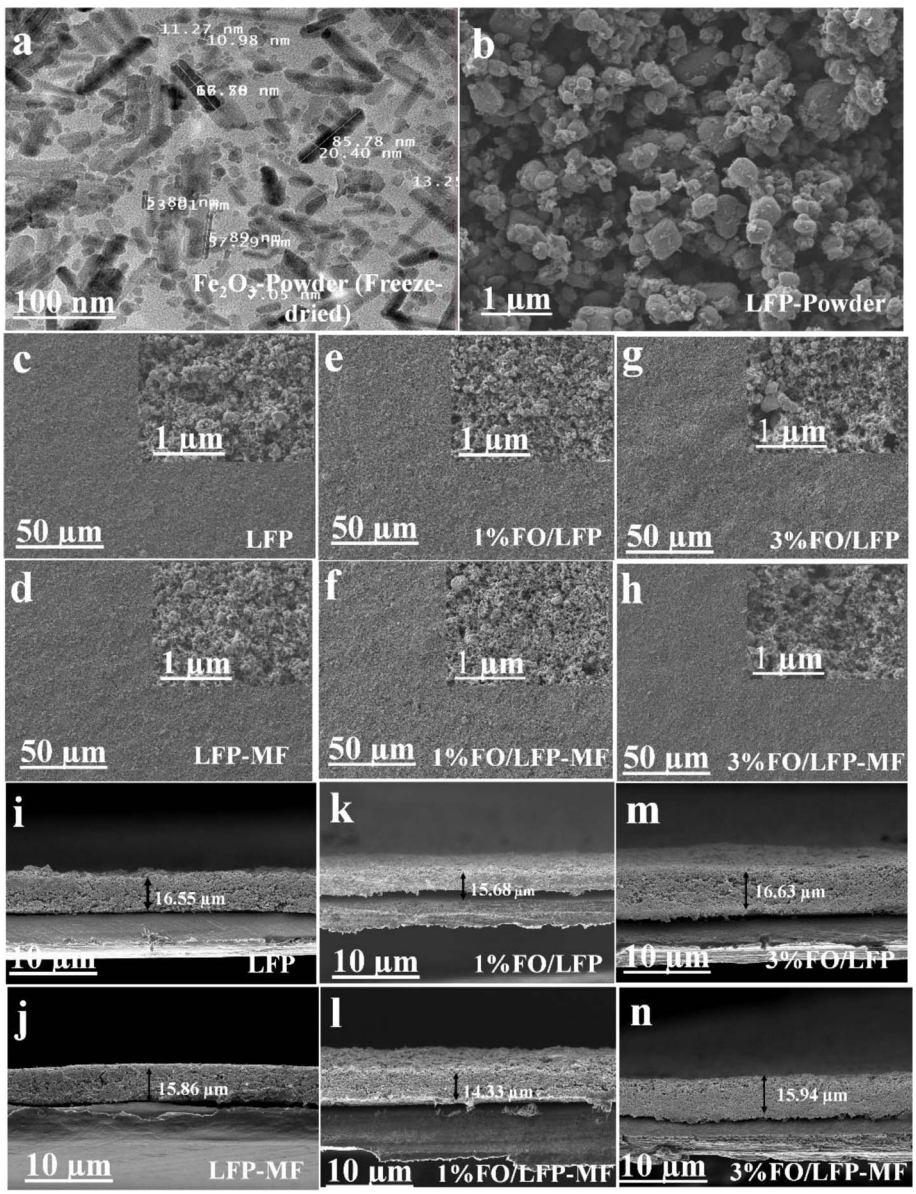

Fig. 2 (a) TEM image of freeze-dried Fe_2O_3 nanoparticles; (b) top-view SEM images of $LiFePO_4$ powder; (c) LFP and (d) LFP-MF; (e) 1% FO/LFP and (f) 1% FO/LFP-MF; and (g) 3% FO/LFP and (h) 3% FO/LFP-MF cathodes; cross-sectional SEM images of cathodes (i) LFP and (j) LFP-MF; (k) 1% FO/LFP and (l) 1% FO/LFP-MF; (m) 3% FO/LFP and (n) 3% FO/LFP-MF.

an amplitude of 10 mV. The LFP cathode prepared with or without magnetic field were investigated using a Hall effect measurement system (HMS-5500, Ecopia Inc., South Korea), with a magnetic field of 0.53 T at a temperature of 297.83 ± 1.72 K. The sample's slurries were doctor blade-coated to a thickness of 20 μm onto a non-conductive polymer-laminated aluminum foil and were cut into 1 × 1 cm samples after drying. The samples were tested at 5 mA and 15 mA (Fig. 6 and S6 (ESI)†).

3. Results and discussions

The crystalline characteristics of the $LiFePO_4$ powder sample and related cathodes, prepared with and without MF, were investigated by XRD (Fig. 1). The significant diffraction peaks of the sample match the $LiFePO_4$ standard pattern, and the absence of any additional peaks suggests that the polycrystalline LFP samples contained no impurities. The LFP (Fig. 1a), 1% FO/LFP (Fig. 1b), and 3% FO/LFP (Fig. 1c) electrodes dried with and without magnet acquire diffraction peaks of the orthorhombic *Pnma* space group, which corresponds to the standard software data (PDF-4$^+$ 2023, JCPDS card no. 01-090-1862, shown in Fig. S1, ESI†). According to the literature data,[4] the preferred growth pattern of particles may be studied by using the intensity ratio $I(020)/I(111)$. A higher ratio than the standard value of 0.87 (from JCPDS card no. 01-090-1862) indicates a layered structure and usually represents preferred orientation along the atomic planes. For LFP-MF, the ratio increases to 0.90, compared to 0.88 for LFP. This shows that magnetic placement causes LFP to position itself perpendicularly to the (020) surface. Considering the ratio of 1% FO/LFP-MF and 3% FO/LFP-MF, it increases to 1.01 and 1.10, respectively, while for 1% FO/LFP and 3% FO/LFP, the values are 0.90 and 0.98. This decrease suggests that the magnetic field (MF) enhances the positioning along the (020) plane; this also affects the electrode compactness.

TEM was used to analyze the particle size of Fe_2O_3, with the results shown in Fig. 2. These measurements revealed an average FO nanoparticle size of approximately 91.18 ± 2.26 nm, showcasing rod-shaped and spherical morphologies. Further, SEM was conducted to examine the morphology of the $LiFePO_4$ cathode powder, and the possible effect of MF on the electrode thickness. At first, we checked the possible morphological changes by top-view SEM imaging. From Fig. 2b, it was observed that the particles in the initial $LiFePO_4$ powder are spherical, with evenly dispersed grains. Further, Fig. 2c and d show the top-view SEM image of the LFP and LFP-MF cathodes, while Fig. 2e and f demonstrate 1% FO/LFP and 1% FO/LFP-MF cathodes, and Fig. 2g and h show the top-view SEM images of 3% FO/LFP and 3% FO/LFP-MF cathodes. The images reveal that the cathode powders were well mixed with carbon in composite electrodes. No difference could be observed in the top-view images of all electrodes subjected to MF and without MF because the polycrystalline nature of the particles does not allow tracking their rotation like in the case of single-crystal particles or nanosheets.[1] Next, we investigated the changes in the cross-sectional thickness of all electrodes by SEM. As shown in Fig. 2i and j, the cross-sectional SEM images of the electrodes

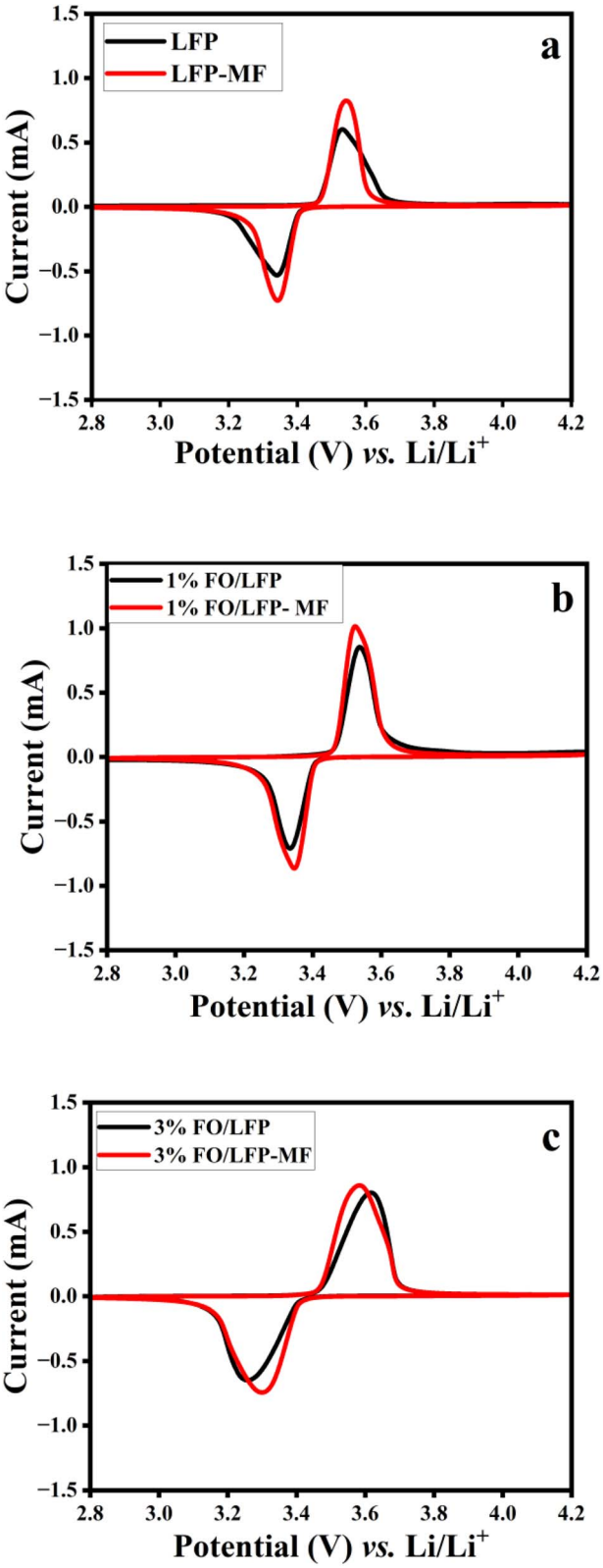

Fig. 3 (a) CV scans (4th cycle) of LFP and LFP-MF; (b) 1% FO/LFP and 1% FO/LFP-MF; and (c) 3% FO/LFP and 3% FO/LFP-MF.

revealed the cathode thickness for LFP to be 16.55 μm with a standard mean error (SME) of 0.54 μm, while LFP-MF had a smaller thickness of 15.85 ± 0.82 μm. Fig. 2k and l show the

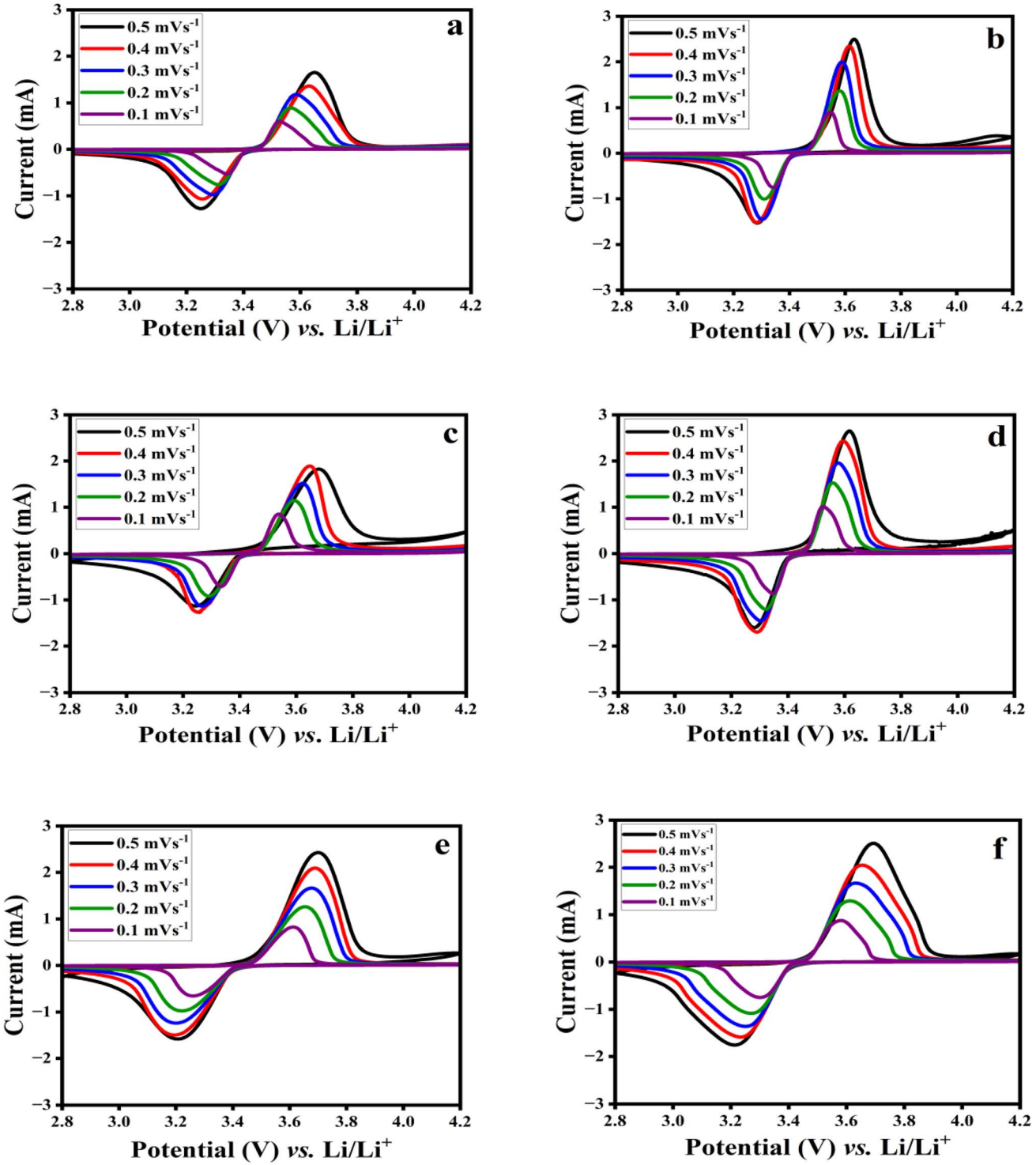

Fig. 4 CV curves at various rates from 0.1 to 0.5 mV s^{-1} for (a) LFP, (b) LFP-MF, (c) 1% FO/LFP, (d) 1% FO/LFP-MF, (e) 3% FO/LFP, and (f) 3% FO/LFP-MF.

thickness of 1% FO/LFP 15.68 ± 0.70 μm, while for 1% FO/LFP-MF, it was around 14.33 ± 0.71 μm. In Fig. 2m and n, the cathode thickness of 3% FO/LFP is measured at 16.63 ± 0.88 μm, while 3% FO/LFP-MF electrodes show a thickness of 15.94 ± 0.98 μm. Despite the thicknesses for the samples with/without MF overlap within the SME, it can be seen that the MF treatment affects the cathode thickness. Notably, there is a consistent trend across the different electrode compositions, with the cathodes treated with MF exhibiting reduced thickness compared to those without MF. The mechanism behind this phenomenon could be possibly attributed to the fact that the magneto-sensitive particles (FO) and LFP may be pulled towards

the bottom of the electrode by a MF. This process could shrink the thickness of the electrode, forming a one-dimensional channel through which Li^+ can move and diffuse more easily, therefore, enhancing the porosity of the electrode. This effect turned out to be significant for 1% FO-MF, resulting in a lower thickness, but was not pronounced for 3% FO-MF. The reasons for such a phenomenon require further investigation, including other electrode materials, such as $LiCoO_2$ and, probably, some other 'less paramagnetic' materials, to further clarify and distinguish the role of the magnetic particle additives (FO) in compacting the electrode.

The above-mentioned results emphasize the significance of the MF treatment and FO in affecting the electrodes' structural properties, which could have implications for the overall performance and efficiency of the battery.

The CV experiments were performed to investigate the MF effect on the electrochemical performance of the electrodes. The potential peak position differences (ΔV) between the oxidation and reduction peaks were calculated using the data from the fourth cycle of each cell to evaluate the performance variation due to the magnetic field effect.[4] All electrodes displayed distinct reversible redox peaks (Fig. 3) corresponding to the electrochemical transformation of Fe^{2+}/Fe^{3+} phases, indicating highly reversible Li^+ deintercalation and intercalation processes.[5,22,23] As shown in Fig. 3a–c, the LFP-MF, 1% FO/LFP-MF, and 3% FO/LFP-MF electrodes exhibit notable anodic peaks at 3.53, 3.52 and 3.58 V (*vs.* Li/Li^+ for all electrochemical measurements) and cathodic peaks around 3.34, 3.33, and 3.29 V, respectively. The cathodic and anodic peak differences (ΔV) of the electrodes, which also reflect the kinetic polarization upon REDOX processes, in this case, were 0.19, 0.18, and 0.29 V, respectively. This is lower than that of non-MF counterparts LFP (0.20 V), 1% FO/LFP (0.22 V), and 3% FO/LFP (0.36 V). The prominent anodic peaks of LFP, 1% FO/LFP, and 3% FO/LFP occurred at 3.54, 3.55, and 3.61 V, while the cathodic peaks occurred at 3.34, 3.33, and 3.25 V. It should be noted that a lower ΔV indicates enhanced electrode kinetics and reversibility, thus reflecting lower electrochemical polarization.[4] The higher CV test activity of the cells with MF can be attributed to the influence of magnetic placement on the macrostructure and particle packing of the polycrystalline LFP material during the electrode preparation, such as particle orientation, their denser particle packing, and requiring shorter Li ion diffusion in a thinner electrode. These effects led to an enhanced electrochemical performance, including a stronger CV response. Further increasing the additive content increases the polarization, which slows down the electrode's kinetics, affecting its performance negatively. Therefore, these results imply that the electrodes, dried under MF, exhibit improved electrode kinetics, reversibility, and slower capacity deterioration during long-term cycling, as shown in Fig. S5,† while exhibiting higher current (which reflects the reaction rate) values than those of all the electrodes prepared without magnetic field (WMF).

Following the CV-confirmed evidence of positive MF's effects on the FO/LFP electrode kinetics, the diffusion coefficients for the studied systems were estimated to confirm the impact of MF on the electrode operation. The diffusion coefficient was estimated based on the CV measurements at scan rates ranging from 0.5 to 0.1 mV s^{-1}. The results of these investigations are presented in Fig. 4 and Table 1. Notably from Fig. 4, as the scan rate increases, distinct redox peaks arise in the CV profiles of the electrodes, thus indicating a rise in the electrochemical reaction rate. At the same time, the redox peaks potential difference increases as well (Fig. S2a–c, ESI†), showing that the electrode polarization rises. The Randles–Sevcik equation was used to determine the diffusion coefficient of Li^+ (D_{Li^+}) for the electrodes.[24] From Fig. 4a, the LFP displays a decrease in the current peaks and a diffusion coefficient of 2.14×10^{-4} cm^2 s^{-1} compared with LFP-MF (Fig. 4b) that has a higher current peak and diffusion coefficient of 4.14×10^{-4} cm^2 s^{-1} (Fig. S2a, ESI†). As per Fig. 4c and d, the diffusion coefficient of the 1% FO/LFP cathode is 2.45×10^{-4} cm^2 s^{-1}, which is lower than that of 1% FO/LFP-MF (4.06×10^{-4} cm^2 s^{-1}, Fig. S2b, ESI†). Further, Fig. 4e shows that 3% FO/LFP exhibits a slight decrease in the current peaks and a lower diffusion coefficient of 1.32×10^{-4} cm^2 s^{-1} compared with 3% FO/LFP-MF (2.30×10^{-4} cm^2 s^{-1}) in Fig. 4f and S2c (ESI).† However, all the electrodes dried under MF exhibited superior electrochemical properties and higher lithium diffusion coefficients (Table 1) than those of the WMF electrodes (dried without MF). These results confirm that a magnetic field treatment could enhance the Li^+ movement by improving the lithium diffusion kinetics and the overall performance of the battery.

Further, the EIS analysis was utilized to assess the effect of MF on the charge transfer resistance of the electrodes. Fig. 5 shows the Nyquist plots for all cathodes after the 5th CV cycle for all electrodes scanned at 0.1 mV s^{-1}. All EIS spectra consist of a semicircle in the high- to medium-frequency range and a straight line in the low-frequency range. The first semicircle in the high- to medium-frequency region is attributed to R_1 and Q elements in the equivalent circuit (Fig. 5), where R_1 represents particle-to-particle and particle-to-collector contact resistances, while R_2 signifies the charge-transfer resistance between the electrolyte and the active material. Q represents the constant phase element (CPE), and W (Q_3) denotes a Warburg impedance primarily associated with the Li^+ diffusion within the bulk electrode.[4,5] From the EIS data, all cathodes dried under MF exhibited lower charge transfer resistances than those of the WMF cathode. Thus, the circuit's total resistance is primarily determined by the sum of R_2 and R_1. After fitting using the Biologic (EC-Lab software, V11.60), the R_2 values of LFP-MF, 1%

Table 1 Diffusion coefficient ($D_{Li^+}{}^{0.5}$) data and EIS fitting parameters of charge-transfer resistance (R_2)

	Li^+ diffusion coefficient (cm^2 s^{-1})		Charge-transfer resistance (R_2) after the 5th CV scan (ohm)	
Sample	Bare	MF	Bare	MF
LFP	2.14×10^{-4}	4.14×10^{-4}	35.79	31.44
1% FO/LFP	2.45×10^{-4}	4.06×10^{-4}	20.52	18.64
3% FO/LFP	1.32×10^{-4}	2.30×10^{-4}	45.51	30.40

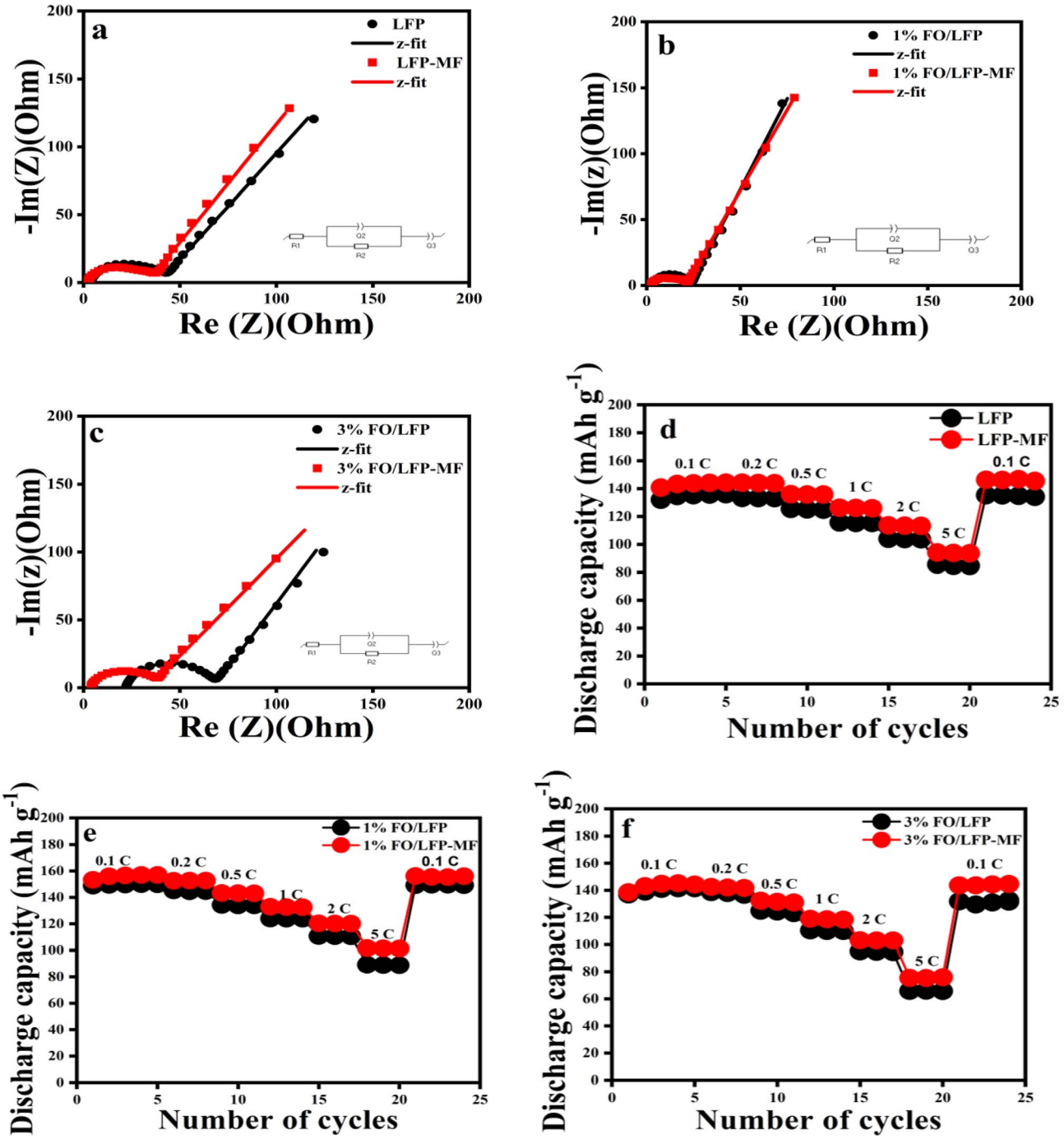

Fig. 5 (a) Nyquist plots of AC impedance spectra for LFP and LFP-MF; (b) 1% FO/LFP and 1% FO/LFP-MF; and (c) 3% FO/LFP and 3% FO/LFP-MF. Comparison of the rate capacity data for (d) LFP and LFP-MF; (e) 1% FO/LFP and 1% FO/LFP-MF; and (f) 3% FO/LFP and 3% FO/LFP-MF.

FO/LFP-MF, and 3% FO/LFP-MF samples were determined to be 31.44, 18.64, and 30.40 Ω, respectively. Comparatively, the internal resistance of LFP, 1% FO/LFP, and 3% FO/LFP samples was higher than those placed on a magnetic field, as seen in Table 1. The higher internal resistance observed in the 3% FO/LFP compared to the 1% FO/LFP electrode can be attributed to the low conductivity of FO, and probably caused by recurrent electrode expansion/shrinkage due to a thermal release or Li^+ insertion/de-insertion within the multilayer structure for the electrode.[4] In the case of the electrode samples dried under a magnetic field, the electrochemical impedance decreases during cycling *versus* the WMF electrodes due to reduced polarization. These results indicated that MF could improve the reaction kinetics, resulting in a higher rate capability and enhanced performance of the electrode materials.

The galvanostatic charge–discharge performance of the cathodes was assessed to comprehensively investigate any changes in their electrochemical behavior caused by the

magnet's placement during the preparation of the cathode. Fig. S4a–c (ESI)† depicts the charge–discharge profiles for all electrodes at 0.1 and 0.2C rates and 4.2–2.8 V cutoff potentials for the 4th cycle. The 4th cycle was selected because the cell performance stabilizes during the initial cycles. According to the data in Fig. S4a–c (ESI),† the specific discharge capacities for LFP, 1% FO/LFP, and 3% FO/LFP at 0.1C were 150.2, 148.8, and 144.3 mA h g^{-1}, respectively, which are slightly lower than those of LFP-MF (152.0 mA h g^{-1}), 1% FO/LFP-MF (150.0 mA h g^{-1}), and 3% FO/LFP-MF (148.6 mA h g^{-1}). At a higher cycling rate of 0.2C, the capacity gap between two batches of samples became slightly more obvious, with the electrodes placed under a magnetic field showing a higher discharge capacity. Further, Fig. S5 (ESI)† shows a prolonged cycling performance of 1% FO/LFP-MF at 0.2C over 100 cycles. The results confirm the stability and durability of the electrode material in extended cycling with excellent capacity retention.

Furthermore, the electrochemical performance of $LiFePO_4$ electrodes was investigated at different C rates. Fig. 5d–f shows the rate capability of the electrodes, and it can be seen that the electrodes dried under MF had a higher reversible capacity and a slower capacity degradation compared to their counterparts. Expectedly, the capacity of all electrodes (with and without MF) decreases as the charge–discharge rate rises due to the kinetics limitations. Although there is no obvious difference between the discharge capacities of LFP electrodes placed under MF and WMF at a rate less than 1C, as observed in Fig. 5d–f, the significant variations become evident at a higher discharge rate. At 1C, the discharge capacities of LFP-MF, 1% FO/LFP-MF, and 3% FO/LFP-MF were approximately 9.21, 7.01, and 7.73% higher than WMF-electrodes. At 2C, LFP-MF exhibited a 9.25% higher capacity, while 1% FO/LFP-MF and 3% FO/LFP-MF showed minor improvements of 8.78% and 9.02%, respectively, compared with the WMF-electrode samples. At 5C, all the LFP electrodes with MF displayed higher discharge capacities than the WMF-electrode, with increases of 10.65% for LFP-MF, 15.90% for 1% FO/LFP-MF, and 15.63% for 3% FO/LFP-MF. It can be seen that the cells with the electrode containing 1% FO had the highest average capacity at a rate of 5C. This implies that 1% FO concentration functions with a less negative effect at this loading. As a result, a notable difference in discharge capacities between LFP electrodes placed under MF and WMF at higher charge–discharge rates is probably due to the severe polarization induced by a high current. This effect, enhanced by the magnetic field during the drying process, influences the overall performance of the battery system and contributes to the observed differences in discharge capacities. LFP-MF electrodes have an accelerated Li^+ diffusion, accompanied by increased discharge capacities, slower capacity decay, and high reversibility at high rates compared to LFP without magnet placement.

The effect of the magnetic field and FO on the conductivity of the obtained LFP cathode samples was investigated using Hall effect measurements, as presented in Fig. 6. The highest conductivity, 1.12 S cm^{-1}, was observed for the 1% FO/LFP-MF sample, optimizing the electron transport. The differences in conductivity values for the LFP samples are shown in Fig. 6.

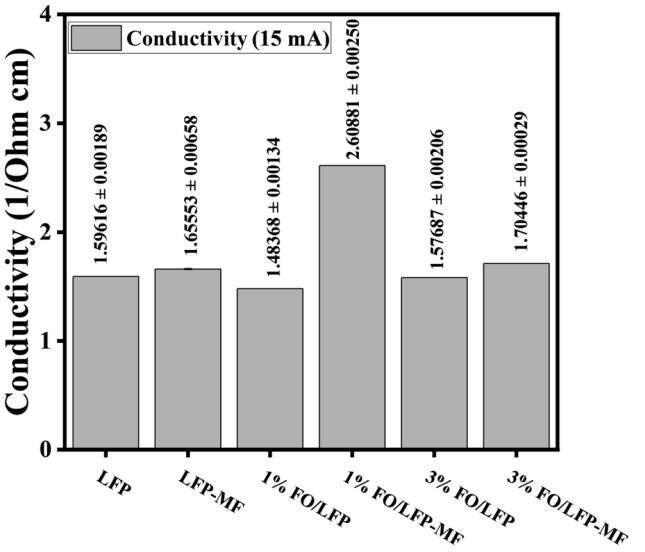

Fig. 6 Hall effect measurement results of LFP, 1% FO/LFP and 3% FO/LFP samples with/without MF at 5 mA.

However, when the FO percentage increased to 3%, the conductivity worsened, indicating that excess FO impairs electron transport.

Thus, the FO additive enhances the electrochemical performance of $LiFePO_4$ cathodes, both with and without the application of a magnetic field. Despite observing no significant changes in the morphology or crystalline characteristics following SEM and XRD analyses (Fig. 1 and 2), the electrodes prepared under the magnetic field exhibited not only higher density but also improved pathways for Li ion migration, crucial for enhancing the battery performance, while the electrodes prepared without MF appeared thicker and loosen, with randomly dispersed Li ion migration paths. Further, the electrodes with 1% FO/LFP benefited from enhanced FO infusion under a magnetic field, resulting in improved electrochemical performance. However, the electrodes containing 3% FO/LFP experienced a decrease in their performance, supposedly, due to the FO low electrical and ionic conductivity, which may have affected the network necessary for efficient Li ion insertion/deinsertion. This phenomenon worsens charge transfer resistance, as evidenced by our EIS measurements (Fig. 5c), thereby impeding the electrode's charge and discharge kinetics. Therefore, while $LiFePO_4$ cathodes with MF-assisted FO incorporation could enhance the electrode density and Li ion pathways, the electrical and ionic conductivities of FO play a critical role in determining the electrochemical performance and efficiency of the electrode in practical battery applications.

4. Conclusion

In this study, Fe_2O_3 powder was added into commercial $LiFePO_4$ at two concentrations to prepare composite cathodes, which were dried with and without the application of MF of 0.3 T. From the XRD results, it can be observed that this modification of the preparation process with MF did not alter the fundamental structural characteristics of the cathode materials. The

SEM observations revealed consistent morphology of the electrodes, and reduced electrode thickness for the samples prepared 'with MF', which potentially enhanced the porosity of the electrodes for improved Li-ion diffusion and battery performance. The CV experiments confirmed that the MF-treated electrodes displayed lower polarization and higher currents of electrochemical reactions, indicating improved electrode kinetics and lithium diffusion compared to non-MF-treated electrodes. Based on the obtained EIS spectra, LFP-MF, 1% FO/LFP-MF, and 3% FO/LFP-MF show a lower charge transfer resistance than that of the counter electrodes, which were not affected by MF during drying. According to the results obtained from the electrochemical tests, the electrodes placed under the MF upon drying showed improved electrochemical characteristics and suppressed polarization, thus contributing to a superior electrochemical performance of battery. However, there was no obvious difference between the discharge capacities of LFP subjected to MF and WMF electrodes at a cycling rate less than 1C. In contrast, the batteries with the electrode containing 1% FO exhibited the highest average capacity at a rate of 5C, which implies that 1% FO additive functions better under these conditions.

The advantageous effect of MF during electrode preparation significantly enhanced the electrochemical performance of the cathodes. Employing MF to enhance the Li-ion diffusion and electrochemical kinetics of the reactions in $LiFePO_4$ leads to increased discharge capacities and enhanced stability even at high cycling rates. The findings of this study demonstrate that MF-treated cathodes exhibit enhanced electrochemical performance compared to those prepared without MF, resulting in reduced polarization, enhanced Li-ion diffusion, and improved capacity retention. This research highlights a relatively facile method to improve the rate capability of the commercial $LiFePO_4$ cathodes that can be incorporated into the large-scale battery production.

Data availability

The data supporting this article have been included as part of the ESI.†

Author contributions

Emmanuel Iheonu Nduka: investigations, methodology, data collection, writing – original draft. Mukagali Yegamkulov: investigation, data collection. Nazgul Assan: investigations, methodology, data collection, validation, writing – review and editing. Aliya Mukanova: conceptualization, validation, writing – review and editing. Zhumabay Bakenov: supervision, funding acquisition, conceptualization, validation, resources, writing – review & editing.

Conflicts of interest

The authors state that they have no known competing financial interests or personal relationships that could have impacted the research provided in this paper.

Acknowledgements

The authors acknowledge the financial support of the Program Targeted Funding BR21882402 "Development of new material technologies and energy storage systems for a green economy" from the Ministry of Science and Higher Education of the Republic of Kazakhstan and the Research Grant 0122022FD4136 "Combined effect of magnetic field and ultrasound waves on fast-charging lithium-ion batteries" from Nazarbayev University.

References

1 D. Gao, J. Yang, D. Zhang and C. Chang, An effective strategy to enhance the electrochemical performance of $LiNi_{0.6}Mn_{0.2}Co_{0.2}O_2$: optimizing a Li diffusion pathway via magnetic alignment of single-crystal cathode material under an ordinary 0.4-T magnetic field, *Ceram. Int.*, 2022, **48**(21), 31598–31605.
2 K. Shen, X. Xu and Y. Tang, Recent progress of magnetic field application in lithium-based batteries, *Nano Energy*, 2022, **92**, 106703.
3 Z. Chen, Q. Zhang and Q. Liang, Carbon-Coatings Improve Performance of Li-Ion Battery, *Nanomaterials*, 2022, **12**, 1936.
4 J. Zhou, D. Zhang, G. Sun and C. Chang, B-axis oriented alignment of $LiFePO_4$ monocrystalline platelets by magnetic orientation for a high-performance lithium-ion battery, *Solid State Ionics*, 2019, **338**, 96–102.
5 C. Kim, Y. Yang, D. Ha, D. H. Kim and H. Kim, Crystal alignment of a $LiFePO_4$ cathode material for lithium ion batteries using its magnetic properties, *RSC Adv.*, 2019, **9**(55), 31936–31942.
6 N. Bai, H. Chen, W. Zhou, K. Xiang, Y. Zhang, C. Li, *et al.*, Preparation and electrochemical performance of $LiFePO_4$/C microspheres by a facile and novel co-precipitation, *Electrochim. Acta*, 2015, **167**, 172–178.
7 D. Li, X. Liu and H. Zhou, The Size-Dependent Phase Transition of $LiFePO_4$ Particles during Charging and Discharging in Lithium-Ion Batteries, *Energy Technol.*, 2014, **2**(6), 542–547.
8 Y. Gao, K. Chen, H. Chen, X. Hu, Z. Deng and Z. Wei, Surfactant assisted solvothermal synthesis of $LiFePO_4$ nanorods for lithium-ion batteries, *J. Energy Chem.*, 2017, **26**(3), 564–568.
9 N. Bai, K. Xiang, W. Zhou, H. Lu, X. Zhao and H. Chen, $LiFePO_4$/carbon nanowires with 3D nano-network structure as potential high performance cathode for lithium ion batteries, *Electrochim. Acta*, 2016, **191**, 23–28.
10 Y. Hu, G. Wang, C. Liu, S. L. Chou, M. Zhu, H. Jin, *et al.*, $LiFePO_4$/C nanocomposite synthesized by a novel carbothermal reduction method and its electrochemical performance, *Ceram. Int.*, 2016, **42**(9), 11422–11428.
11 Q. f. Zhao, Y. h. Yu, Q. s. Ouyang, M. y. Hu, C. Wang, J. h. Ge, *et al.*, Surface Modification of $LiFePO_4$ by Coatings for Improving of Lithium-ion Battery Properties, *Int. J. Electrochem. Sci.*, 2022, **17**, 221142.

12 G. Yang, K. Pan, F. Lai, Z. Wang, Y. Chu, S. Yang, *et al.*, Integrated co-modification of PO_4^{3-} polyanion doping and Li_2TiO_3 coating for Ni-rich layered $LiNi_{0.6}Co_{0.2}Mn_{0.2}O_2$ cathode material of lithium-ion batteries, *Chem. Eng. J.*, 2021, **421**, 129964.

13 Y. Zou, G. Chang, S. Chen, T. Liu, Y. Xia, C. Chen, *et al.*, Alginate/r-GO assisted synthesis of ultrathin $LiFePO_4$ nanosheets with oriented (0 1 0) facet and ultralow antisite defect, *Chem. Eng. J.*, 2018, **351**, 340–347.

14 W. W. Yang, J. G. Liu, X. Zhang, L. Chen, Y. Zhou and Z. G. Zou, Ultrathin $LiFePO_4$ nanosheets self-assembled with reduced graphene oxide applied in high rate lithium ion batteries for energy storage, *Appl. Energy*, 2017, **195**, 1079–1085.

15 N. A. Chernova, G. M. Nolis, F. O. Omenya, H. Zhou, Z. Li and M. S. Whittingham, What can we learn about battery materials from their magnetic properties?, *J. Mater. Chem.*, 2011, **21**(27), 9865–9875.

16 Y. Sun, S. Zhang, W. Yuan, Y. Tang, J. Li and K. Tang, Applicability study of the potting material based thermal management strategy for permanent magnet synchronous motors, *Appl. Therm. Eng.*, 2019, **149**, 1370–1378.

17 W. C. Chien, K. N. Liu, S. C. Chang and C. C. Yang, Effects of α-Fe_2O_3 size and morphology on performance of $LiFePO_4$/C cathodes for Li-ion batteries, *Thin Solid Films*, 2018, **660**, 931–937.

18 S. Wu, Y. Jin, D. Wang, Z. Xu, L. Li, X. Zou, *et al.*, Fe_2O_3/carbon derived from peanut shell hybrid as an advanced anode for high performance lithium ion batteries, *J. Energy Storage*, 2023, **68**, 107731.

19 J. Guo, M. Lan, S. Wang, Y. He, S. Zhang, G. Xiang, *et al.*, Enhanced saturation magnetization in buckypaper-films of thin walled carbon nanostructures filled with Fe_3C, FeCo, FeNi, CoNi, Co and Ni crystals: the key role of Cl, *Phys. Chem. Chem. Phys.*, 2015, **17**(27), 18159–18166.

20 Y. Wang, H. Li, M. Chen, X. Yang and D. Jiang, Synthesis and electrochemical performance of $LiFePO_4$/C cathode materials from Fe_2O_3 for high-power lithium-ion batteries, *Ionics*, 2017, **23**(2), 377–384.

21 H. M. Cheng, F. M. Wang and J. P. Chu, Effect of Lorentz force on the electrochemical performance of lithium-ion batteries, *Electrochem. Commun.*, 2017, **76**, 63–66.

22 L. Yang, J. Chen, L. Chen, P. Yang, J. Zhang, A. Li, *et al.*, $LiFePO_4$ nanoplates with {010} exposed active planes prepared by hydrothermal method, *J. Mater. Sci.: Mater. Electron.*, 2016, **27**(11), 12258–12263.

23 J. M. Tarascon and M. Armand, Issues and challenges facing rechargeable lithium batteries, *Nature*, 2001, **414**, 359–367.

24 Y. Hu, D. Gu, H. Jiang, L. Wang, H. Sun, J. Wang, *et al.*, Electrochemical Performance of LiFePO/C via Coaxial and Uniaxial Electrospinning Method, *Adv. Chem. Eng. Sci.*, 2016, **6**(2), 149–157.